System size effects on the free energy landscapes from molecular dynamics of phase-separating bilayers

Ashlin J. Poruthoor,[1] Jack J. Stallone,[1] Megan Miaro,[1] Akshara Sharma,[1] and Alan Grossfield[1, a)]
Department of Biochemistry and Biophysics, University of Rochester Medical Center, Rochester, NY 14642

(Dated: 14 June 2024)

The "lipid raft" hypothesis proposes that cell membranes contain distinct domains of varying lipid compositions, where "rafts" of ordered lipids and cholesterol coexist with disordered lipid regions. Experimental and theoretical phase diagrams of model membranes have revealed multiple coexisting phases. Molecular dynamics (MD) simulations can also capture spontaneous phase separation of bilayers. However, these methods merely determine the sign of the free energy change upon phase separation — whether or not it is favorable — but not the amplitude. Recently, we developed a workflow to compute the free energy of phase separation from MD simulations using the weighted ensemble method. However, while theoretical treatments generally focus on infinite systems and experimental measurements on mesoscopic to macroscopic systems, MD simulations are comparatively small. Thus, if we are to put the results of these calculations into the appropriate context, we need to understand the effects the finite size of the simulation has on the computed free energy landscapes. In this study, we investigate this phenomenon by computing free energy profiles for a model phase-separating system as a function of system size, ranging from 324 to 10,110 lipids. The results indicate that the free energy difference appears to converge once the system reaches approximately 8000 lipids.

I. INTRODUCTION

Cell membranes are often compositionally heterogeneous, spontaneously forming domains exhibiting collective behavior and preferential interactions[1–5]. The formation of such functional domains has been attributed to liquid-liquid phase separation, which can be recapitulated in simple model membranes[6–10]. However, the biological importance of phase separation in membranes and the size, lifetime, biochemical makeup, and functional importance of the resulting domains has been debated for many years[11–14]. Recent studies have proposed an adaptable fluid mosaic model for biological membranes, spatially tuned to reside close to a critical point so that the phase separation can be used for functional roles[15,16].

Due to their high spatial and temporal resolution, molecular dynamics (MD) simulations have been used extensively to study phase separation in lipid mixtures and augment the experimental results[17–23]. Although all-atom MD simulations studies of lipid phase separation have been reported[24–30], previous studies have predominantly used coarse-grained models to minimize the computational expense. This was necessary because capturing phase separation requires a relatively large simulation. While spontaneous separation may occur on time scales accessible to MD, estimating the thermodynamic favorability of the process would require a significant number of reversible transitions, which is prohibitively slow. To circumvent this limitation, we developed FLOPSS[31], a workflow built on the weighted ensemble method[32–34] to compute the membrane phase separation thermodynamics from MD by enhancing the sampling[35] along a novel clustering-based collective variable.

[a)]Electronic mail: alan_grossfield@urmc.rochester.edu

Systematic errors can arise while estimating thermodynamic quantities from simulations due to the finite size of the simulation box[36]. Previous studies have explored the system-size effect on computing transport properties such as translational diffusion coefficients and viscosities[37–40], on free energies of solvation[41], and nucleation[42] from MD simulations. Such finite-size effects are also well-documented for lipid bilayer systems[43–48]. Thus, it is necessary to know the extent and meaning of fluctuations and correlated motions within the system and how they affect the computed bulk properties[49]. Ideally, a simulation would be large enough to approach the thermodynamic limit, where the bulk-like behavior is independent of the extent of the system. Recently, a systematic study of finite-size effects on the domain formation in a ternary lipid bilayer using standard MD simulation with systems ranging from 240 to 5406 lipids suggested a lower limit for macroscale domain formation and estimated that the thermodynamic limit would require systems of 10,000 lipids or more[50]. A similar conclusion was reached in a study applying Monte Carlo sampling to a lattice model of lipid mixtures[51,52].

Inspired by these studies, we use molecular dynamics simulations to investigate finite-size effects on the free energy landscapes of a phase-separating ternary lipid bilayer. The ternary lipid bilayer that we investigate consists of dipalmitoylphosphatidylcholine (DPPC), dilinoleylphosphatidylcholine (DIPC), and cholesterol (CHOL), at a molar ratio of 0.42:0.28:0.3. We use the FLOPSS workflow to estimate the free energy landscapes of forming distinct domains in this system as a function of system size ranging from 324 lipids to 10110 lipids while keeping the lipid composition and hydration the same. We track the evolution of these free energy curves and $\Delta\Delta G_{\text{sep}}$ with system size, and show that for this system both appear to converge once the bilayers contain approximately 8000 lipids.

II. METHODS

As reported previously[31], FLOPSS is a workflow to compute the free energy landscapes of phase-separating systems which we tested on multiple ternary lipid bilayer systems simulated at varying temperatures. The workflow starts with building the bilayer replicates, followed by running standard MD simulations. These standard simulations are then used to collect seed configurations for weighted ensemble MD simulations to enhance the sampling of mixing and demixing the bilayer. In our original FLOPSS study, we showed that the choice of progress coordinate is not trivial and can lead to misleading conclusions due to poor convergence. We reported that a progress coordinate based on the clustering of lipids can be an excellent choice. In this study, we applied the same protocol to DPPC-DIPC-CHOL systems of varying sizes, using the coordinate designated as FLC_{opt} in our original work.

A. System Construction and Standard MD Simulation

Using the MARTINI-MAKER module from CHARMM-GUI[53], we built DPPC-DIPC-CHOL systems, in a molar ratio of 0.42:0.28:0.3, with varying sizes ranging from 324 to 10110 lipids; see Table I for a complete listing of systems. For each system size, we built 4 independent replicates. MARTINI 2.x particle parameters and force field parameters[54,55] were used, along with MARTINI polarizable water[56]. An approximate 1:30 lipid:real water ratio was maintained in all systems. Following the CHARMM-GUI Martini Maker default protocol, each system was minimized and equilibrated in steps using the GROMACS 2020.3 package[57]. However, to prevent the excessive membrane undulations that were previously reported to be associated with large membrane systems[58–60], we applied a flat-bottomed restraint potential[61] with a well radius of 2.3125 nm and force constant $k = 1000$ KJ mol^{-1}nm^{-2} to the PO4 beads of phosphatidylcholine lipids.

All production simulations were performed using GROMACS 2020.3. Unless otherwise mentioned, we have adopted previously reported MARTINI simulation parameters[62]. For Van der Waals interaction, a potential-shift van der Waal's modifier was used with a 1.1 nm cutoff. For electrostatics, we used the reaction field method[63] with a 1.1 nm coloumb cutoff and a dielectric constant = 2.5 is used. The verlet cutoff scheme[64] with a neighbor list update frequency of 20 time steps was used for neighbor searching. The extended-ensemble Parrinello-Rahman pressure coupling[65] was used with a 12 ps time constant, a compressibility of 3×10^{-4} bar^{-1}, and 1 bar reference pressure. Velocity rescaling[66] with a 1 ps time constant was used for temperature coupling. For better accuracy and energy conservation, we used the LINCSolver constraint coupling matrix[67] with 8^{th} order expansion and short 20 fs timesteps respectively[68]. These choices were based on previous reports of artifacts due to inaccurate constraints in MARTINI coarse-grained bilayer simulations. For all replicates, an initial 100 ns run at 400K in the NPT ensemble was followed by two independently forked 4 μs standard MD production runs, at 323K and 423K respectively. The low-temperature runs were used to sample the phase separated state and transitional values, while the 423K remained mixed. The short high-temperature run at the beginning was intended to ensure random mixing of lipids at the starting state, since some demixing occurred during the equilibration process.

B. Choice of Progress Coordinate

A progress coordinate or collective variable is intended to represent the complex multidimensional dynamics of the system in a single dimension that is easy to track and interpret. Thus, for the same system, a progress coordinate can vary depending on the question one is addressing. Frequently, progress coordinates are used to track the progress of the transition of interest in a system, which in our case is the transition of the bilayer from a mixed state to a separated state and vice versa. Progress coordinates are also central to the application of many enhanced sampling techniques, including the weighted ensemble method at the core of the FLOPSS workflow[34,69]. Previously, we have reported that progress coordinates that correlate with phase separation in bilayers often do not enhance the sampling in WE simulations. We identified one effective choice, the Fraction of Lipids in Clusters (FLC), defined as

$$\text{FLC} = \frac{\sum_i^N \text{No. of Lipid X}_i \text{ in Lipid X}_i \text{ Clusters}}{\text{Total No. of Lipids}} \qquad (1)$$

where subscript i denotes the individual lipid species in a bilayer consisting of N total lipid species. Since we have a ternary DPPC-DIPC-CHOL system, $N = 3$. FLC can range from 0 to 1, where FLC = 1 indicates a separated state where all lipids are part of some cluster. This clustering is performed using the Density-Based Spatial Clustering of Applications with Noise (DBSCAN) algorithm[70,71] as implemented in scikit-learn[72]. We pre-compute all lipid-lipid distances two-dimensionally, treating the two leaflets independently.

DBSCAN takes two parameters: the distance, within which two lipids are considered neighbors, and the minimum number of neighbors needed to form a cluster. In our previous work, we used two different sets of clustering parameters, but here we use the values we previously termed FLC_{opt} in our previous work, as these parameters do a better job of distinguishing mixed and separated states. The optimized set of values for the DPPC-DIPC-CHOL system were (26.5 Å, 24 neighbors), (31.5 Å, 26 neighbors), and (32.5 Å, 23 neighbors) for DPPC, DIPC, and cholesterol respectively.

C. Weighted Ensemble Simulation

Each iteration of the weighted ensemble (WE) algorithm contains 2 components. In the first, a number of "walkers" (conventional MD simulations) are propagated starting from each bin on the progress coordinate. In the second component, the progress coordinate is updated based on the state of

Total number of lipids	No. of DPPC (0.42)	No. of DIPC (0.28)	No. of Cholesterol (0.3)	Total CG Water	Average box dimensions (x × y × z) (*nm*)
324	138	90	96	2430	11.78 × 11.58 × 6.67
648	276	180	192	4860	15.92 × 15.92 × 6.69
972	414	270	288	7290	19.49 × 19.24 × 6.62
1944	828	540	576	14580	26.51 × 26.55 × 6.91
3888	1656	1080	1152	29160	37.09 × 37.04 × 6.88
7776	3312	2160	2304	58320	51.39 × 51.34 × 7.13
10110	4306	2808	2996	75825	58.27 × 58.33 × 7.22

TABLE I. Details of lipid composition, solvation and dimensions of the different systems under study. Average box dimensions are calculated after 4 μs standard MD production run at 323K (Supplementary Table S1)

the system at the end of each walker trajectory, and based on that the walker is assigned to a bin. The target number of walkers per bin is maintained by merging or splitting walkers, while conserving the statistical weight in each bin. More details on the theory and implementation of the weighted ensemble method can be found in recent reviews[34,73].

We ran two replicates of weighted ensemble simulations for each system size. We seeded each replicate by picking evenly spaced frames from the last microsecond of each of the conventional MD simulations. We used structures from both the 323K and 423K simulations to ensure that the weighted ensemble simulations initially sampled both well-mixed and demixed states, to speed equilibration and convergence of the WE simulations.

To propagate the WE simulations, we used WESTPA2 v2022.06[74] and followed the previously established protocols[31,73,75]. A Minimal Adaptive Binning (MAB) scheme[76] was employed to divide the progress coordinate space into 30 dynamic bins. We set the target number of "walkers" per bin to 4. To speed up the convergence of WE simulations, the WE Equilibrium Dynamics (WEED) reweighting protocol[77,78] was used with a reweighting window of 10 iterations. It is not statistically correct to average values across multiple reweighting windows, so unless otherwise noted average values reported here are from the last 10 iterations of the WE simulations. GROMACS 2020.3 was used to propagate the MD part of each iteration using the same settings detailed above.

For all the system sizes except 7778 and 10110 lipids, each replicate completed WE 1000 iterations. The system with 7778 and 10110 lipids completed 600 and 500 iterations respectively, as the computational cost was significantly higher. However, for the systems that ran 1000 iterations, we saw that the results don't change significantly after the first 500 iterations.

All simulations were run using the BlueHive computing cluster in the Center for Integrated Research and Computing facility at the University of Rochester. Intel Xeon E5-2695, Gold 6130, 6140, and 6330 processors with Tesla K20Xm, K80, V100, and A100 GPUs were used to propagate the dynamics.

Simulation data was processed and analyzed with the LOOS software package[79]. The data from each WE replicate was combined using *w_multi_west* tool in WESTPA2. Subsequently, WESTPA2 tools such as *w_pdist* and *plothist* were used to construct the free energy landscapes, $\Delta G(\mathrm{FLC})$. The data generated from WE simulations were projected onto other auxiliary variables to derive further insights using *w_crawl* and LOOS tools.

Once the free energy landscapes were constructed for each system, we calculated the average FLC, $\langle \mathrm{FLC} \rangle$ as given below

$$\langle \mathrm{FLC} \rangle \doteq \frac{\sum(\mathrm{FLC}\ \rho(\mathrm{FLC}))}{\sum \rho(\mathrm{FLC})} \tag{2}$$

where $\rho(\mathrm{FLC})$ is the probability of finding the system at a particular FLC value as obtained from WE. Similarly, we can estimate the variance and standard deviation $\sigma(\mathrm{FLC})$ by using the analogous formula for $\langle \mathrm{FLC}^2 \rangle$. We also quantified the fluctuations in free energy curves by computing the variance $\Delta G(\mathrm{FLC})$ over a range of FLC values. To compute the free energy difference between the mixed and phase-separated states of the system, $\Delta\Delta G_{\mathrm{sep}}$, we identified the maximum value of ΔG within the range $\langle \mathrm{FLC} \rangle \pm \sigma(\mathrm{FLC})$, and considered that to be the barrier between the two states. To distinguish genuine barriers from statistical noise, we only considered the maximum to be a barrier if it was greater than $2\sigma(\Delta G)$.

III. RESULTS

A. Finite Size Effects From Standard MD

Figure 1 shows the evolution of the FLC as a function of time, from standard MD simulations that ran at 323K and 423K, with four independent replicates simulated at each temperature. For all system sizes, the FLC values remain very low at 423K, indicating that the lipids are well-mixed. By contrast, at 323K, the FLC values increase rapidly over the first 100 ns of each trajectory before equilibrating and remaining stable for the remainder of the trajectory, suggesting highly non-ideal mixing and possibly phase separation.

The average FLC values don't appear to vary significantly with system size at either temperature; this is visible in Figure 1 and shown quantitatively in Supplementary Table S2. However, the fluctuations drop significantly as the system size increases, indicating qualitatively different behavior with

different-sized systems. If we track the contribution of individual species to FLC, we see a similar trend, as shown in Supplementary Figure S1.

To better understand the nature of the structural differences with system size, we tracked the size of the clusters formed by individual lipid species. Figure 2 shows the average size of lipid clusters as a function of system size as computed from the standard MD simulations. As expected, large clusters are not observed at the higher temperature. However, at 323K the mean cluster size increases with system size for the smallest systems. However, the average cluster size plateaus, within the limits of the statistical uncertainties, once there are roughly 2000 lipids in the system. This strongly suggests that smaller periodic boxes suppress the formation of larger aggregates.

B. Finite Size Effects on Free Energy Landscapes from Weighted Ensemble Molecular Dynamics

Figure 3 shows the free energy curves obtained from WE MD runs, averaging over the last 10 WE iterations. For the smaller systems, the free energy surfaces are flat and noisy. However, for larger systems than 3888 lipids, the free energy curves are smoother, with well-defined basins at relatively low FLC and high FLC values. This implies that the system can be found in a relatively mixed state (where fewer lipids are part of clusters) as well as a demixed state (where more lipids are part of clusters); based on previous analysis, the construction of the progress coordinate and visual inspection, we interpret the high-FLC basin as the phase-separated one, while the lower-FLC basin is a single-phase but non-ideally mixed state.

For the smaller systems, virtually the entire range $0.2 <$ FLC < 0.8 is thermodynamically accessible. However, for systems with 3888 lipids and larger, the width of the wells narrows, and the free energy increases more rapidly at the edges. For the two largest systems, the free energy curves are very similar.

One key question is whether the system size affects the morphology of the membrane; Figure 2 showed this to be the case using the conventional MD simulations, but WE should allow a more complete exploration of the free energy landscape. Figure 4 shows the distribution of DPPC cluster sizes for all system sizes simulated. Except for the smallest 324-lipid system, the primary peak in the distribution is around 50-60 lipids in a cluster. However, the distribution is far from gaussian, with a significant tail at large cluster sizes. Moreover, all of the distributions have a secondary large-cluster peak, but the location of this peak varies non-monotonically with system size. It is not clear whether this results from statistical noise due to poor convergence as large clusters slowly coalesce, or if this is a genuine feature of the system.

C. Finite Size Effects on $\Delta\Delta G_{\text{sep}}$ Estimation

The free energy difference between the mixed and the demixed states of the system, $\Delta\Delta G_{\text{sep}}$, can be obtained by

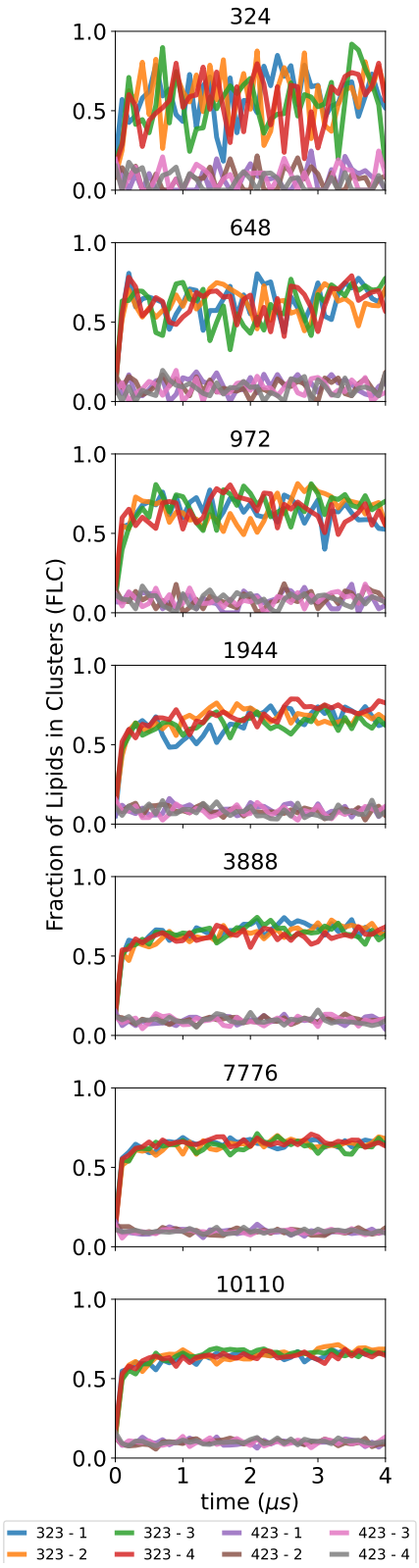

FIG. 1. Evolution of FLC of the system over 4 μs at 323K and 423K. Line colors correspond to independent replicates simulated at different temperatures.

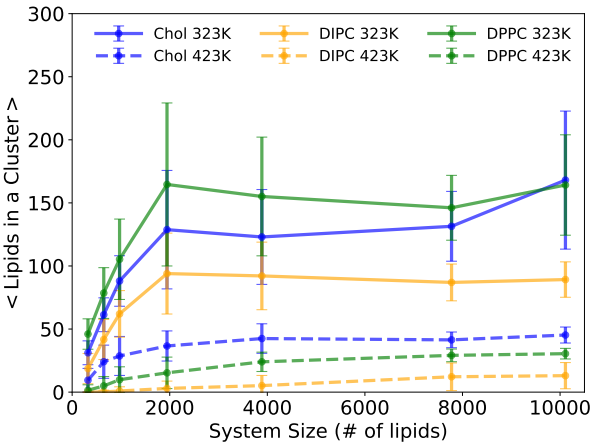

FIG. 2. Average size of lipid clusters as a function of system size. Dashed lines represent the simulations at 423K, while solid lines show the data from the simulations at 323K. The error bars are the standard error computed treating each replica as a single measurement.

defining an FLC cutoff that distinguishes one state from another and using the weights from the WE simulations to compute their relative probabilities:

$$\Delta\Delta G_{\text{sep}} = -k_B T \ln \frac{p_{\text{demixed}}}{p_{\text{mixed}}} \tag{3}$$

The challenge, therefore, is to identify an appropriate cutoff in an unbiased manner. With a smooth two-well free energy curve, the choice is obvious — the local maximum of the free energy is the best choice — but the present curves have sufficient statistical noise to make it necessary to use a more robust procedure. As discussed in the Methods section, we compute the average and standard deviation of FLC from the ΔG curve, and search for the highest local maximum within one standard deviation of the average. To distinguish noise from a genuine barrier, we only consider maxima whose values is greater than $2\,\sigma(\text{FLC})$.

Figure 3 shows that, for the smaller systems, the free energy surfaces are relatively flat and noisy, and do not resemble double-well free energy curves. Although we can apply the above algorithm to calculate a $\Delta\Delta G_{\text{sep}}$ for them, in reality we would argue that phase separation does not occur. For the 3 largest systems (3888, 7776, and 10110 lipids), the free energy curves do show a clear double-well shape; for the latter two, the location of the average and the walls are consistent, and our algorithm identifies similar FLC cutoffs.

The resulting $\Delta\Delta G_{\text{sep}}$ values are shown in Figure 5. The estimated free energy changes are sensitive to the system size, fluctuating non-monotonically for the smaller systems; this is largely an artifact of the flat landscapes making a separation into 2 states somewhat arbitrary. However, for the 3 largest systems, $\Delta\Delta G_{\text{sep}}$ is consistent to within ≈ 0.1 kcal/mol. Consistent with our previous work[31], the values are slightly positive, indicating that the melting temperature for phase separa-

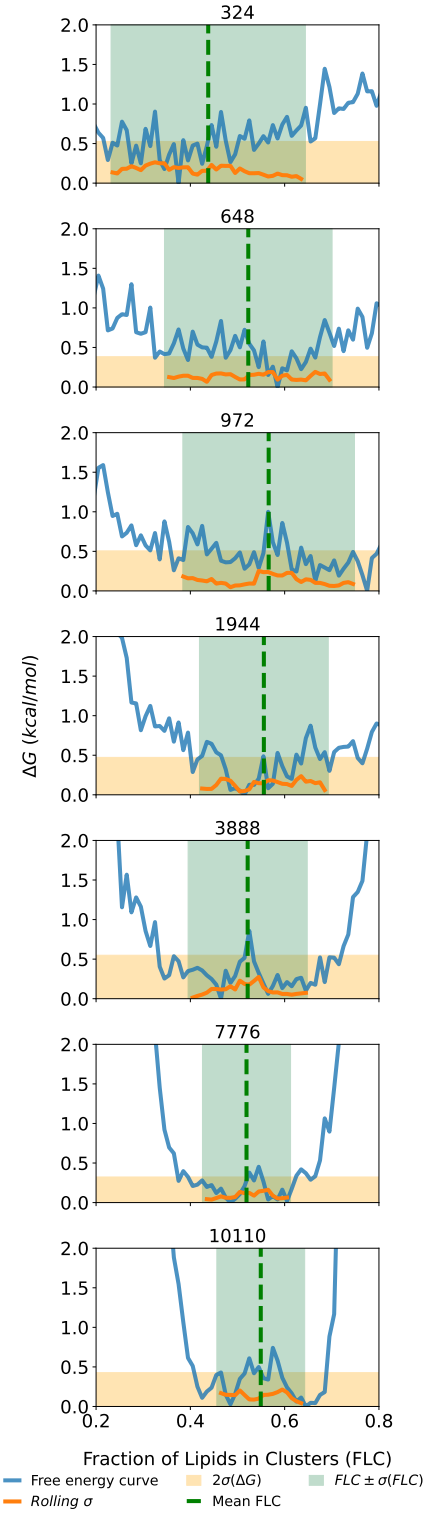

FIG. 3. Free energy landscapes for system sizes varying from 324 to 10110 lipids (blue curves). For each system size, the vertically dotted dark green line indicates the average FLC, $\langle FLC \rangle$, the vertical light green slab indicates $\langle FLC \rangle \pm \sigma(FLC)$, the orange line indicates the running standard deviation, while the horizontal light orange slab corresponds to $2\sigma(\Delta G)$ within the light green slab.

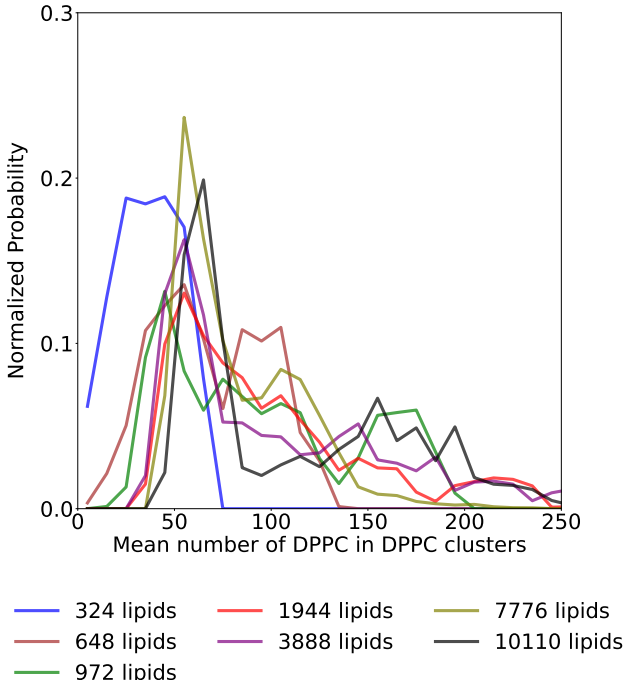

FIG. 4. Probability distribution for DPPC cluster sizes for all system sizes.

tion is roughly 323K. This information would not be accessible from conventional simulations alone.

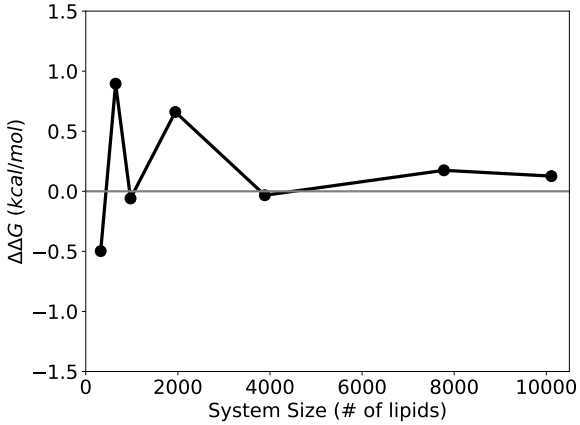

FIG. 5. Computed $\Delta\Delta G_{\text{sep}}$ for systems ranging from 324 lipids to 10110 lipids.

IV. DISCUSSION

Molecular dynamics simulations of lipid bilayers face a fundamental challenge in that they attempt to represent an infinite (or at least macroscopic) system with a finite number of molecules replicated via periodic boundary conditions. In a sense, we go into the calculations knowing that periodic boundaries are "wrong", and while they are clearly the least wrong choice, it is still crucial to understand how the finite size of the system affects the results.

This challenge is particularly acute when studying phase separation in lipid bilayers. The formation of domains is intrinsically a macroscopic or at least mesoscopic phenomenon, while atomistic simulations (even with coarse-grained potentials) are necessarily microscopic. Theoretical approaches generally assume an infinite system, or at least one large enough that the size of the system doesn't affect the results, and tend to break down for smaller systems. Thus, when attempting to compare simulations to experiments or theory, it is important to understand potential finite-size artifacts present in the simulations.

In this work, we leverage our recently developed technology for computing the free energy landscape of lipid phase separation[31] to directly measure these finite-size effects. We conclude that small systems are unable to separate at all, but rather undergo a wide range of fluctuations, as indicated by the wide, flat free energy curves. A barrier between two states begins to emerge with the $\approx$ 2000-lipid systems, and the two largest systems ($\approx$ 8000 and 10000 lipids, respectively) have free energy curves that are consistent within statistical error, while the $\Delta\Delta G_{\text{sep}}$ is consistent once the systems reach about 4000 lipids.

Previous studies have investigated finite-size effects in the simulation of lipid phase separation, although the present work is to our knowledge the first to use the free energy landscape as a readout. For example, Pantelopulos et. al.[50] performed coarse-grained simulations of a lipid composition similar to the one in this paper and tracked a number of order parameters as a function of system size. Although their largest simulation had roughly 5400 lipids, they extrapolated their systems' behavior to estimate that bulk behavior would be observed for systems with 10000 lipids. A previous lattice model simulation of 2-component bilayer phase separation also concluded that 10000 lipid systems were sufficiently large to eliminate finite-size effects[51].

V. CONCLUSIONS

Whenever one tries to draw conclusions from simulations of phase separation (or similar bulk phenomena), one natural question to ask is whether the system is big enough to accurately represent the phenomenon in question. The present work uses the free energy landscape as a readout for the phase separation of a ternary lipid bilayer, measuring its dependence on the size of the simulation. We see that for very small systems, phase separation is entirely suppressed, but once the systems approaches 10^4 lipids, more bulk-like behavior is observed. The present work has 2 limitations. First, using a ternary system means we don't know if the minimum bulk system size will change with the addition of more components, including other lipid species, transmembrane or periph-

eral proteins, etc. Second, it would be ideal to have systems sizes far larger than our estimated threshold for the thermodynamic limit. However, the computational cost of such simulations is currently prohibitively high. As an alternative, we plan to perform analogous calculations using simpler lattice models, which should make calculations across 3-4 orders of magnitude in system size tractable.

SUPPLEMENTARY MATERIAL

See supplementary material for simulation details. It contains further standard MD analysis details including (1) mean and variance of FLC, (2) evolution of individual species contribution to FLC, (3) species-wise cluster count analysis and (4) cluster size. Supplementary material also contains further weighted ensemble analysis such as individual species contribution to free energy landscapes, and species-wise cluster size details.

AUTHOR CONTRIBUTIONS

AJP and AG designed the project. AJP, JJS, MM and AS performed the research. AJP and AG wrote the manuscript.

ACKNOWLEDGEMENTS

The authors thank the Center for Integrated Research Computing (CIRC) at the University of Rochester for providing computational resources and technical support. AJP thanks the Leon Miller Fellowship from the University of Rochester Medical Center. This work was supported by grant R21GM138970 (to AG) from the National Institutes of Health.

DECLARATION OF INTERESTS

The authors have no conflicts of interest.

DATA AVAILABILITY STATEMENT

All analysis scripts, WESTPA configuration scripts, simulation snapshots and source data are made available on GitHub (`https://github.com/Poruthoor/systemSizeEffectsInWEMD`) or upon request.

[1] S. J. Singer and G. L. Nicolson, "The Fluid Mosaic Model of the Structure of Cell Membranes," Science **175**, 720–731 (1972).
[2] K. Simons and E. Ikonen, "Functional rafts in cell membranes," Nature **387**, 569–572 (1997).
[3] M. Edidin, "The state of lipid rafts: From model membranes to cells," Annual Review of Biophysics and Biomolecular Structure **32**, 257–283 (2003).
[4] D. M. Engelman, "Membranes are more mosaic than fluid," Nature **438**, 578–580 (2005).
[5] E. Klotzsch and G. J. Schütz, "A critical survey of methods to detect plasma membrane rafts," Philosophical Transactions of the Royal Society B: Biological Sciences **368**, 20120033 (2013).
[6] S. L. Veatch and S. L. Keller, "Organization in Lipid Membranes Containing Cholesterol," Physical Review Letters **89**, 268101 (2002).
[7] S. L. Veatch and S. L. Keller, "Separation of Liquid Phases in Giant Vesicles of Ternary Mixtures of Phospholipids and Cholesterol," Biophysical Journal **85**, 3074–3083 (2003).
[8] K. Simons and W. L. Vaz, "Model systems, lipid rafts, and cell membranes," Annual Review of Biophysics and Biomolecular Structure **33**, 269–295 (2004).
[9] S. L. Veatch and S. L. Keller, "Seeing spots: Complex phase behavior in simple membranes," Biochimica et Biophysica Acta - Molecular Cell Research **1746**, 172–185 (2005).
[10] S. L. Veatch, S. S. W. Leung, R. E. W. Hancock, and J. L. Thewalt, "Fluorescent Probes Alter Miscibility Phase Boundaries in Ternary Vesicles," The Journal of Physical Chemistry B **111**, 502–504 (2007).
[11] S. Munro, "Lipid Rafts," Cell **115**, 377–388 (2003).
[12] A. K. Kenworthy, "Have we become overly reliant on lipid rafts?" EMBO reports **9**, 531–535 (2008).
[13] E. Sezgin, I. Levental, S. Mayor, and C. Eggeling, "The mystery of membrane organization: composition, regulation and roles of lipid rafts," Nature Reviews Molecular Cell Biology **18**, 361–374 (2017), arXiv:NIHMS150003.
[14] I. Levental, K. R. Levental, and F. A. Heberle, "Lipid Rafts: Controversies Resolved, Mysteries Remain," Trends in Cell Biology **30**, 341–353 (2020).
[15] S. L. Veatch, N. Rogers, A. Decker, and S. A. Shelby, "The plasma membrane as an adaptable fluid mosaic," Biochimica et Biophysica Acta (BBA) - Biomembranes **1865**, 184114 (2023).
[16] S. A. Shelby, I. Castello-Serrano, K. C. Wisser, I. Levental, and S. L. Veatch, "Membrane phase separation drives responsive assembly of receptor signaling domains," Nature Chemical Biology **19**, 750–758 (2023).
[17] R. W. Pastor, R. M. Venable, and S. E. Feller, "Lipid Bilayers, NMR Relaxation, and Computer Simulations," Accounts of Chemical Research **35**, 438–446 (2002).
[18] S. J. Marrink, J. Risselada, and A. E. Mark, "Simulation of gel phase formation and melting in lipid bilayers using a coarse grained model," Chemistry and Physics of Lipids **135**, 223–244 (2005).
[19] J. D. Perlmutter and J. N. Sachs, "Interleaflet Interaction and Asymmetry in Phase Separated Lipid Bilayers: Molecular Dynamics Simulations," Journal of the American Chemical Society **133**, 6563–6577 (2011).
[20] W. D. Bennett and D. P. Tieleman, "Computer simulations of lipid membrane domains," Biochimica et Biophysica Acta (BBA) - Biomembranes **1828**, 1765–1776 (2013).
[21] A. J. Sodt, R. W. Pastor, and E. Lyman, "Hexagonal Substructure and Hydrogen Bonding in Liquid-Ordered Phases Containing Palmitoyl Sphingomyelin," Biophysical Journal **109**, 948–955 (2015).
[22] D. S. Patel, S. Park, E. L. Wu, M. S. Yeom, G. Widmalm, J. B. Klauda, and W. Im, "Influence of Ganglioside GM1 Concentration on Lipid Clustering and Membrane Properties and Curvature," Biophysical Journal **111**, 1987–1999 (2016).
[23] A. Bandara, A. Panahi, G. A. Pantelopulos, and J. E. Straub, "Exploring the structure and stability of cholesterol dimer formation in multicomponent lipid bilayers," Journal of Computational Chemistry **38**, 1479–1488 (2017).
[24] S. A. Pandit, S. Vasudevan, S. Chiu, R. Jay Mashl, E. Jakobsson, and H. Scott, "Sphingomyelin-Cholesterol Domains in Phospholipid Membranes: Atomistic Simulation," Biophysical Journal **87**, 1092–1100 (2004).
[25] G. Khelashvili, B. Kollmitzer, P. Heftberger, G. Pabst, and D. Harries, "Calculating the Bending Modulus for Multicomponent Lipid Membranes in Different Thermodynamic Phases," Journal of Chemical Theory and Computation **9**, 3866–3871 (2013).
[26] A. J. Sodt, M. L. Sandar, K. Gawrisch, R. W. Pastor, and E. Lyman, "The molecular structure of the liquid-ordered phase of lipid bilayers," Journal of the American Chemical Society **136**, 725–732 (2014).
[27] M. Javanainen, H. Martinez-Seara, and I. Vattulainen, "Nanoscale Membrane Domain Formation Driven by Cholesterol," Scientific Reports **7**, 1143 (2017).
[28] R.-X. X. Gu, S. Baoukina, D. P. Tieleman, and D. Peter Tieleman, "Phase Separation in Atomistic Simulations of Model Membranes," Journal of the American Chemical Society **142**, 2844–2856 (2020).

[29]S. W. Canner, S. E. Feller, and S. R. Wassall, "Molecular Organization of a Raft-like Domain in a Polyunsaturated Phospholipid Bilayer: A Supervised Machine Learning Analysis of Molecular Dynamics Simulations," The Journal of Physical Chemistry B **125**, 13158–13167 (2021).
[30]S. Dehghani-Ghahnaviyeh, M. Smith, Y. Xia, A. Dousis, A. Grossfield, and S. Sur, "Ionizable Amino Lipids Distribution and Effects on DSPC/Cholesterol Membranes: Implications for Lipid Nanoparticle Structure," The Journal of Physical Chemistry B **127**, 6928–6939 (2023).
[31]A. J. Poruthoor, A. Sharma, and A. Grossfield, "Understanding the free-energy landscape of phase separation in lipid bilayers using molecular dynamics," Biophysical Journal **122**, 4144–4159 (2023).
[32]G. A. Huber and S. Kim, "Weighted-ensemble Brownian dynamics simulations for protein association reactions," Biophysical Journal **70**, 97–110 (1996).
[33]B. W. Zhang, D. Jasnow, and D. M. Zuckerman, "The "weighted ensemble" path sampling method is statistically exact for a broad class of stochastic processes and binning procedures," The Journal of Chemical Physics **132**, 054107 (2010).
[34]D. M. Zuckerman and L. T. Chong, "Weighted Ensemble Simulation: Review of Methodology, Applications, and Software," Annual Review of Biophysics **46**, 43–57 (2017).
[35]J. Henin, T. Lelievre, M. R. Shirts, O. Valsson, and L. Delemotte, "Enhanced Sampling Methods for Molecular Dynamics Simulations [Article v1.0]," Living Journal of Computational Molecular Science **4**, 1–60 (2022), arXiv:2202.04164.
[36]V. Privman, *Finite Size Scaling and Numerical Simulation of Statistical Systems* (WORLD SCIENTIFIC, 1990).
[37]M. Mondello and G. S. Grest, "Viscosity calculations of n-alkanes by equilibrium molecular dynamics," Journal of Chemical Physics **106**, 9327–9336 (1997).
[38]M. Fushiki, "System size dependence of the diffusion coefficient in a simple liquid," Physical Review E - Statistical Physics, Plasmas, Fluids, and Related Interdisciplinary Topics **68**, 6 (2003).
[39]I.-C. Yeh and G. Hummer, "System-Size Dependence of Diffusion Coefficients and Viscosities from Molecular Dynamics Simulations with Periodic Boundary Conditions," The Journal of Physical Chemistry B **108**, 15873–15879 (2004).
[40]T. Iwashita, M. Nagao, A. Yoshimori, M. Terazima, and R. Akiyama, "Usefulness of higher-order system-size correction for macromolecule diffusion coefficients: A molecular dynamics study," Chemical Physics Letters **807**, 140096 (2022).
[41]V. Gapsys and B. L. de Groot, "On the importance of statistics in molecular simulations for thermodynamics, kinetics and simulation box size," eLife **9** (2020), 10.7554/eLife.57589.
[42]M. N. Joswiak, N. Duff, M. F. Doherty, and B. Peters, "Size-Dependent Surface Free Energy and Tolman-Corrected Droplet Nucleation of TIP4P/2005 Water," The Journal of Physical Chemistry Letters **4**, 4267–4272 (2013).
[43]J. B. Klauda, B. R. Brooks, A. D. MacKerell, R. M. Venable, and R. W. Pastor, "An ab Initio Study on the Torsional Surface of Alkanes and Its Effect on Molecular Simulations of Alkanes and a DPPC Bilayer," The Journal of Physical Chemistry B **109**, 5300–5311 (2005).
[44]J. B. Klauda, B. R. Brooks, and R. W. Pastor, "Dynamical motions of lipids and a finite size effect in simulations of bilayers," Journal of Chemical Physics **125** (2006), 10.1063/1.2354486.
[45]M. Roark and S. E. Feller, "Molecular Dynamics Simulation Study of Correlated Motions in Phospholipid Bilayer Membranes," The Journal of Physical Chemistry B **113**, 13229–13234 (2009).
[46]B. A. Camley, M. G. Lerner, R. W. Pastor, and F. L. H. Brown, "Strong influence of periodic boundary conditions on lateral diffusion in lipid bilayer membranes," The Journal of Chemical Physics **143** (2015), 10.1063/1.4932980.
[47]J. J. Harris, G. A. Pantelopulos, and J. E. Straub, "Finite-Size Effects and Optimal System Sizes in Simulations of Surfactant Micelle Self-Assembly," The Journal of Physical Chemistry B **125**, 5068–5077 (2021).
[48]Z. Jarin, O. Agolini, and R. W. Pastor, "Finite-Size Effects in Simulations of Peptide/Lipid Assembly," Journal of Membrane Biology **255**, 437–449 (2022).
[49]E. Braun, J. Gilmer, H. B. Mayes, D. L. Mobley, J. I. Monroe, S. Prasad, and D. M. Zuckerman, "Best Practices for Foundations in Molecular Simulations [Article v1.0]," Living Journal of Computational Molecular Science **1**, 1–28 (2019).
[50]G. A. Pantelopulos, T. Nagai, A. Bandara, A. Panahi, and J. E. Straub, "Critical size dependence of domain formation observed in coarse-grained simulations of bilayers composed of ternary lipid mixtures," The Journal of Chemical Physics **147**, 095101 (2017).
[51]J. Huang and G. W. Feigenson, "Monte Carlo simulation of lipid mixtures: finding phase separation," Biophysical Journal **65**, 1788–1794 (1993).
[52]Z. Zhang, M. Laradji, H. Guo, O. G. Mouritsen, and M. J. Zuckermann, "Phase behavior of pure lipid bilayers with mismatch interactions," Physical Review A **45**, 7560–7567 (1992).
[53]Y. Qi, H. I. Ingólfsson, X. Cheng, J. Lee, S. J. Marrink, and W. Im, "CHARMM-GUI Martini Maker for Coarse-Grained Simulations with the Martini Force Field," Journal of Chemical Theory and Computation **11**, 4486–4494 (2015).
[54]S. J. Marrink, H. J. Risselada, S. Yefimov, D. P. Tieleman, and A. H. de Vries, "The MARTINI Force Field: Coarse Grained Model for Biomolecular Simulations," The Journal of Physical Chemistry B **111**, 7812–7824 (2007).
[55]D. H. de Jong, G. Singh, W. F. D. Bennett, C. Arnarez, T. A. Wassenaar, L. V. Schäfer, X. Periole, D. P. Tieleman, and S. J. Marrink, "Improved Parameters for the Martini Coarse-Grained Protein Force Field," Journal of Chemical Theory and Computation **9**, 687–697 (2013).
[56]S. O. Yesylevskyy, L. V. Schäfer, D. Sengupta, and S. J. Marrink, "Polarizable Water Model for the Coarse-Grained MARTINI Force Field," PLoS Computational Biology **6**, e1000810 (2010).
[57]M. J. Abraham, T. Murtola, R. Schulz, S. Páll, J. C. Smith, B. Hess, E. Lindahl, and E. Lindah, "GROMACS: High performance molecular simulations through multi-level parallelism from laptops to supercomputers," SoftwareX **1-2**, 19–25 (2015).
[58]H. I. Ingólfsson, M. N. Melo, F. J. van Eerden, C. Arnarez, C. A. Lopez, T. A. Wassenaar, X. Periole, A. H. de Vries, D. P. Tieleman, and S. J. Marrink, "Lipid Organization of the Plasma Membrane," Journal of the American Chemical Society **136**, 14554–14559 (2014).
[59]X. Lin and A. A. Gorfe, "Understanding Membrane Domain-Partitioning Thermodynamics of Transmembrane Domains with Potential of Mean Force Calculations," The Journal of Physical Chemistry B **123**, 1009–1016 (2019).
[60]J. Su, S. J. Marrink, M. N. Melo, and A. M. Grossfield, "Localization Preference of Antimicrobial Peptides on Liquid-Disordered Membrane Domains," Frontiers in Cell and Developmental Biology **8**, 1–11 (2020).
[61]M. Abraham, A. Alekseenko, C. Bergh, C. Blau, E. Briand, M. Doijade, S. Fleischmann, V. Gapsys, G. Garg, S. Gorelov, G. Gouaillardet, A. Gray, M. E. Irrgang, F. Jalalypour, J. Jordan, C. Junghans, P. Kanduri, S. Keller, C. Kutzner, J. A. Lemkul, M. Lundborg, P. Merz, V. Miletić, D. Morozov, S. Páll, R. Schulz, M. Shirts, A. Shvetsov, B. Soproni, D. van der Spoel, P. Turner, C. Uphoff, A. Villa, S. Wingbermühle, A. Zhmurov, P. Bauer, B. Hess, and E. Lindahl, "GROMACS 2023 Manual," (2023).
[62]D. H. de Jong, S. Baoukina, H. I. Ingólfsson, and S. J. Marrink, "Martini straight: Boosting performance using a shorter cutoff and GPUs," Computer Physics Communications **199**, 1–7 (2016).
[63]W. F. Van Gunsteren, H. J. Berendsen, and J. A. Rullmann, "Inclusion of reaction fields in molecular dynamics: Application to liquid water," Faraday Discussions of the Chemical Society **66**, 58–70 (1978).
[64]L. Verlet, "Computer "Experiments" on Classical Fluids. I. Thermodynamical Properties of Lennard-Jones Molecules," Physical Review **159**, 98–103 (1967).
[65]M. Parrinello and A. Rahman, "Polymorphic transitions in single crystals: A new molecular dynamics method," Journal of Applied Physics **52**, 7182–7190 (1981).
[66]G. Bussi, D. Donadio, and M. Parrinello, "Canonical sampling through velocity rescaling." The Journal of chemical physics **126**, 14101 (2007), arXiv:0803.4060.
[67]B. Hess, H. Bekker, H. J. C. Berendsen, and J. G. E. M. Fraaije, "LINCS: A linear constraint solver for molecular simulations," Journal of Computational Chemistry **18**, 1463–1472 (1997).
[68]S. Thallmair, M. Javanainen, B. Fábián, H. Martinez-Seara, and S. J. Marrink, "Nonconverged Constraints Cause Artificial Temperature Gradients in Lipid Bilayer Simulations," The Journal of Physical Chemistry B **125**, 9537–9546 (2021).

[69]G. Fiorin, M. L. Klein, and J. Hénin, "Using collective variables to drive molecular dynamics simulations," Molecular Physics **111**, 3345–3362 (2013).

[70]X. X. Martin Ester, Hans-Peter Kriegel, Jiirg Sander, "A Density-Based Algorithm for Discovering Clusters in Large Spatial Databases with Noise," In Proceedings of the 2nd ACM International Conference on Knowledge Discovery and Data Mining (KDD) , 226–231 (1996).

[71]E. Schubert, J. Sander, M. Ester, H. P. Kriegel, and X. Xu, "DBSCAN Revisited, Revisited," ACM Transactions on Database Systems **42**, 1–21 (2017).

[72]E. Pedregosa, F. Varoquaux, G. Gramfort, A. Michel, V. Thirion, B. Grisel, O. Blondel, M. Prettenhofer, P. Weiss, R. and Dubourg, V. Vanderplas, J. Passos, A. Cournapeau, D. Brucher, M.Perrot, M. Duchesnay, "Scikit-learn: Machine Learning in Python," J. Mach. Learn. Res. **12**, 2825–2830 (2011).

[73]A. T. Bogetti, J. M. G. Leung, J. D. Russo, S. Zhang, J. P. Thompson, A. S. Saglam, D. Ray, R. C. Abraham, J. R. Faeder, I. Andricioaei, J. L. Adelman, M. C. Zwier, D. N. LeBard, D. M. Zuckerman, and L. T. Chong, "A Suite of Advanced Tutorials for the WESTPA 2.0 Rare-Events Sampling Software [Article v2.0]," Living Journal of Computational Molecular Science **5** (2022), 10.33011/livecoms.5.1.1655.

[74]J. D. Russo, S. Zhang, J. M. G. Leung, A. T. Bogetti, J. P. Thompson, A. J. DeGrave, P. A. Torrillo, A. J. Pratt, K. F. Wong, J. Xia, J. Copperman, J. L. Adelman, M. C. Zwier, D. N. LeBard, D. M. Zuckerman, and L. T. Chong, "WESTPA 2.0: High-Performance Upgrades for Weighted Ensemble Simulations and Analysis of Longer-Timescale Applications," Journal of Chemical Theory and Computation **18**, 638–649 (2022).

[75]A. T. Bogetti, B. Mostofian, A. Dickson, A. J. Pratt, A. S. Saglam, P. O. Harrison, J. L. L. Adelman, M. Dudek, P. A. Torrillo, A. J. DeGrave, U. Adhikari, M. C. Zwier, D. M. Zuckerman, and L. T. Chong, "A Suite of Tutorials for the WESTPA Rare-Events Sampling Software [Article v1.0]," Living Journal of Computational Molecular Science **1**, 1–32 (2019).

[76]P. A. Torrillo, A. T. Bogetti, and L. T. Chong, "A Minimal, Adaptive Binning Scheme for Weighted Ensemble Simulations," The Journal of Physical Chemistry A **125**, 1642–1649 (2021).

[77]D. Bhatt, B. W. Zhang, and D. M. Zuckerman, "Steady-state simulations using weighted ensemble path sampling," The Journal of Chemical Physics **133**, 014110 (2010).

[78]E. Suárez, S. Lettieri, M. C. Zwier, C. A. Stringer, S. R. Subramanian, L. T. Chong, and D. M. Zuckerman, "Simultaneous Computation of Dynamical and Equilibrium Information Using a Weighted Ensemble of Trajectories," Journal of Chemical Theory and Computation **10**, 2658–2667 (2014), arXiv:1210.3094.

[79]T. D. Romo, N. Leioatts, and A. Grossfield, "Lightweight object oriented structure analysis: Tools for building tools to analyze molecular dynamics simulations," Journal of Computational Chemistry **35**, 2305–2318 (2014).